Faraday Discussions

Accepted Manuscript

This manuscript will be presented and discussed at a forthcoming Faraday Discussion meeting. All delegates can contribute to the discussion which will be included in the final volume.

Register now to attend! Full details of all upcoming meetings: http://rsc.li/fd-upcoming-meetings

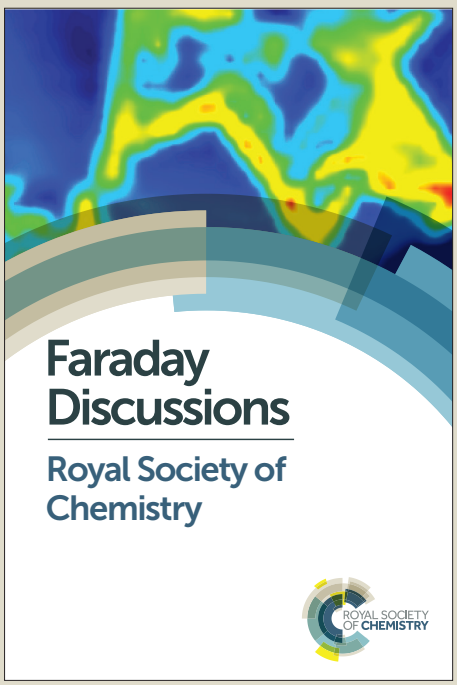

This is an *Accepted Manuscript*, which has been through the Royal Society of Chemistry peer review process and has been accepted for publication.

Accepted Manuscripts are published online shortly after acceptance, before technical editing, formatting and proof reading. Using this free service, authors can make their results available to the community, in citable form, before we publish the edited article. We will replace this *Accepted Manuscript* with the edited and formatted *Advance Article* as soon as it is available.

You can find more information about *Accepted Manuscripts* in the Information for Authors.

Please note that technical editing may introduce minor changes to the text and/or graphics, which may alter content. The journal's standard Terms & Conditions and the Ethical guidelines still apply. In no event shall the Royal Society of Chemistry be held responsible for any errors or omissions in this *Accepted Manuscript* or any consequences arising from the use of any information it contains.

ROYAL SOCIETY OF CHEMISTRY

www.rsc.org/faraday_d

Soft-shear Induced Phase-Separated Nanoparticle String-Structures in Polymer Thin Films

Ren Zhang[1], *Bongjoon Lee*[2], *Michael R. Bockstaller*[2], *Abdullah M. Al-Enizi*[3], *Ahmed Elzatahry*[4,5], *Brian C. Berry*[6], *and Alamgir Karim*[1*]

[1]Department of Polymer Engineering, the University of Akron, 250 S Forge St, Akron, OH 44325

[2]Department of Materials Science and Engineering, Carnegie Mellon University, 5000 Forbes Ave, Pittsburgh, PA 152133

[3]Chemistry Department, Faculty of Science, King Saud University, PO Box 2455, Riyadh 11451, Saudi Arabia

[4]Materials Science and Technology Program, College of Arts and Sciences, Qatar University, PO Box 2713, Doha, Qatar.

[5]Polymer Materials Research Department, Advanced Technology and New Materials Research Institute, City of Scientific Research and Technology Applications, New Borg El-Arab City, Alexandria 21934, Egypt.

[6]Department of Chemistry and Applied Science Program, University of Arkansas at Little Rock, College of Arts, Letters & Sciences, 2801 S University Avenue, Little Rock, AR 72204

[*]Corresponding author: Alamgir Karim (330) 972-8324, alamgir@uakron.edu

Abstract: Application of shear stress has been shown to unidirectionally orient the microstructures of block copolymers and polymer blends. In the present work, we study the phase separation of a novel nanoparticle (NP) – polymer blend thin film system under shear using soft-shear dynamic zone annealing (DZA-SS) method. The nanoparticles are densely grafted with polymer chains of chemically dissimilar composition from the matrix polymer, which induces phase separation upon thermal annealing into concentrated nanoparticle domains. We systematically examine the influence of DZA-SS translation speed and thus the effective shear rate on nanoparticle domain elongation and compare with the counterpart binary polymer blends behavior. Unidirectional aligned nanoparticle string-domains are fabricated with the presence of soft-shear in confined thin film geometry. We expect this DZA-SS method to be applicable to various NP-polymer blends towards unidirectional aligned nanoparticle structures, important to functional nanoparticle structure fabrications.

Key words: nanoparticle, polymer blend thin film, zone annealing, shear rate, phase separation, string morphology.

Polymer-nanoparticle (NP) hybrid materials attracted extensive research interest in nanotechnology since they offer a unique opportunity to engineer novel materials resulting from the combination of nanoscale properties of NPs and the mechanical properties and processability of polymer materials. With various novel nanoparticle synthesis and functionalization techniques, precisely designed polymer grafted nanoparticles are promising building blocks towards versatile nanoparticle structures with advanced photonic, electronic, optical and magnetic properties.[1-5] Polymer grafted nanoparticles have been embedded in a wide range of polymer matrices and the distribution of NPs was successfully manipulated. For instance, nanoparticles were selectively segregated in phase-separated block copolymer template[6,7] or supramolecular frameworks;[8] "self-corralled" nanoparticle superlattice was generated by unfavorable enthalpic interactions between polymer brush and a chemically dissimilar polymer matrix; [9] jamming morphology was observed for NP filled phase-separated polymer blends.[10,11] One simple example of NP-polymer blend is the case where the grafted polymer ligand is composed of the same chemical composition as the free polymer matrix chain, which is the so-called "athermal" blends. In this situation, the dispersion behavior of nanoparticles in homopolymer matrix is determined by relative NP size to free polymer chains, grafting density, and the ratio of the degree of polymerization of polymer matrix and brush.[12,13] Generally, the dispersion of nanoparticles is promoted when the nanoparticle size is smaller than the radius of the gyration of the free polymer chains because of the reduced elastic stretching of polymer matrix chains and the enhanced translation entropy of the nanoparticles.[13,14]

Nanoparticle-polymer blend systems where the grafted polymer chains are of chemically dissimilar compositions from the polymer matrix were less studied, yet the enthalpic interactions between the grafted and free polymer chains can potentially be utilized to control the assembly

structures of nanoparticles. As has been demonstrated in binary polymer blend films, diverse phase-separated morphologies were observed depending on the composition and annealing conditions.[15,16] More importantly, to fabricate novel functional materials such as photonic bandgap materials, nanostructured solar cells, and high-density magnetic storage media, it is essential to control nanoparticle assembled structures. We have previously demonstrated that soft-shear dynamic zone annealing (DZA-SS) process is an efficient way to fabricate unidirectional aligned structures of phase-separated block copolymers (BCPs) and NP-BCP blend films. [17,18] The shear stress during DZA-SS process is generated by local thermal expansion and contraction of a confining soft elastomer capping layer (as it traverses the temperature gradient) at the polymer film surface, which is termed as "soft shear". The more significant deformation of the elastomer capping layer defining the shear direction occurs in the direction of DZA thermal gradient or sample motion direction rather than the orthogonal direction, which generates unidirectional aligned phase separated BCP structures together with nanoparticles. In this study, we investigated a novel binary thin film system composed of densely grafted gold nanoparticles with polystyrene (PS, $M_{n,PS}$ = 11.5 kg/mol) ligands (hereafter denoted as AuPS) and low molecular mass poly(methyl methacrylate) (PMMA, $M_{n,PMMA}$ = 3.1 kg/mol) homopolymer matrix. The average radius of the gold core (R_0) is 1.21 nm and the PS grafting density is 0.7/nm^2. The unfavorable interaction between PMMA matrix and PS brush results in phase-separated morphologies where AuPS nanoparticles formed discrete domains in PMMA matrix while the well-dispersed state of NPs is maintained within the domain structures. DZA-SS induced oscillatory soft-shear was applied to these AuPS/PMMA blend films at various conditions and compared with binary PS/PMMA blend films with $M_{n,PS}$ = 11.5 kg/mol. The correlation between translation speed (v) during DZA-SS process and the deformation

morphology was established considering a conceptual "effective shear rate" ($\dot{\gamma}_E$). Stabilization of highly elongated AuPS "string" morphology was achieved due to shear flow and finite size effect, beyond expected balance of elastic restoring interfacial tension of the nanoparticle domain against the elongating shear flow. Further, prior to coalescence into lines, the nanoparticle domains line-up on average in straight-line fashion presumably to reduce frictional/hydrodynamic interactions between multi nanoparticle domains.

Results and Discussion

The initial distribution state of AuPS nanoparticles in PMMA matrix was examined by top-view transmission electron microscopy (TEM) as shown in Figure 1a. This random in-plane dispersion of nanoparticles induced by good solubility of AuPS in toluene solvent provided a well-defined initial state. Upon vacuum oven annealing at 180 ^{o}C for 16 h, which is significantly higher than the glass transition temperatures (T_g) of both PS ($T_{g\ \mathrm{PS}} \approx 90$ °C) and PMMA ($T_{g\ \mathrm{PMMA}} \approx 105$ °C), the 20% AuPS/PMMA blend films demonstrated a phase separated morphology. As shown in Figure 1b, the AuPS nanoparticles segregated together and formed discrete circular domains in PMMA matrix. It is worth noting that even in these phase-separate domains, the nanoparticles are in a well-dispersed state without aggregation or crystallization. The surface morphology of the phase-separated AuPS/PMMA blend films were characterized by atomic force microscopy (AFM). As demonstrated in Figure 2a and 2b, both PMMA and AuPS phases were observed at the smooth film surface with root-mean-square roughness $R_{rms} \approx 0.76$ nm. By comparison, the phase-separated morphology of 20% PS/PMMA blend films was studied where the molecular weight of the linear PS chains was the same as the grafted PS chains ($M_{n,PS}$ = 11.5kg/mol). Figure 2c and 2d show the AFM height and phase images of this binary polymer blends where similar phase separated morphology was observed with circular PS domains in

PMMA matrix. The film surface is also smooth with $R_{rms} \approx 1.83$ nm. This analogous phase separation behavior of AuPS/PMMA blends and binary polymer blend stems from the common thermodynamic driving force. In both cases, it is the unfavorable enthalpic interaction (Flory-Huggins interaction parameter $\chi_{PS\text{-}PMMA} \sim 0.037$[19], 180 ^{o}C) that drives the phase separation process, considering that the sufficiently high grafting density of the nanoparticles effectively shields the Au cores.[20] The major difference between AuPS/PMMA and PS/PMMA phase-separated structures is that the phase separation scale and average domain size (S) of binary polymer blends is significantly larger compared to NP-polymer blends, which might be correlated to the collective higher viscosity of the densely grafted AuPS nanoparticles [21] as well as configuration difference of the nanoparticle grafted PS chains.

To exert control over the phase-separated structures of these blend films and achieve symmetry breaking of the isotropic circular domains, shear stress was applied to these blend films though soft-shear dynamic zone annealing (DZA-SS) process. As schematically illustrated in Figure 3, the as cast AuPS/PMMA blend film on quartz substrate is laminated with a smooth poly (dimethyl siloxane) (PDMS) capping layer. This assembly is translated across the in-plane temperature gradient profile defined by cold-hot-cold zones. The translation speed (v) ranging from 1 μm/s to 140 μm/s is prescribed by a programmed movable arm. The maximum temperature is controlled at $T_{max} \approx 180$ °C. When the PDMS confined blend film is translated across the thermal gradient field and the temperature rises above T_g, the expansion and contraction of the PDMS generates shear stress in the sample translation direction at the surface of NP-polymer blend film. This drives simultaneous phase separation and NP-domain elongation. As the confined blend films is subjected to temperature rise and fall centered around T_{max}, the shear stress increases and decreases accordingly, composing an oscillatory shear cycle. The shear

rate ($\dot{\gamma}$) variation induced by shear stress (τ) change is dependent on the thermal gradient field, which is controlled and same for all the blend films in the current study. However, the final blend film morphology can be effectively tuned by changing the sample translation speed (v) utilizing the synergistic interaction between phase separation kinetics and the oscillatory shear rate ($\dot{\gamma}$).

The influence of translation speed v during DZA-SS process on final phase-separated morphology of 20% AuPS/PMMA blend films is demonstrated in Figure 4a. Clearly, the AuPS domain deformation is enhanced in the soft-shear direction as v increases from 1 μm/s to 60 μm/s. At a low translation speed of 1μm/s, the circular AuPS domains were slightly deformed with an average aspect ratio (AR) of 1.43 (Table 1), with no spatial distribution preference of the nanoparticle domains. The domain shapes and in-plane arrangement was almost the same as in the vacuum oven annealed case (Figure 1). As v is increased to 20 μm/s, the average AuPS domain size decreased slightly ($S \approx 0.053$ μm^2) and the elongation of nanoparticle domains became more pronounced with $AR = 2.5$. Interestingly, the AuPS domains were lined up in soft-shear direction, forming a "necklace-like" structure. Further increase in speed (v = 40 μm/s and 60 μm/s) resulted in coexistence of small discrete drops ($S \approx 0.02$ μm^2) and highly elongated nanoparticle domains in soft-shear direction. This extremely elongated morphology under high shear rate is referred to as "strings". [22] The domains are also roughly aligned in straight lines on average, suggestive of a minimization of their friction/hydrodynamic interactions between domains. In all above cases, the initial high dispersion of nanoparticles retained after the DZA-SS process (Figure 4b). Previous studies have shown formation of necklace of particles in viscoelastic fluid under shear flow, which was attributed to normal stress effects. [23,24] Particle alignment was generated at low volume factions, indicating enhanced hydrodynamic interactions

in viscoelastic fluid. For Newtonian polymer blends, Migler et al.[25] also reported a "necklace" structure during a droplet-string morphology transition. Aligning of the phase-separated polymer blend domains was observed when the droplet size was comparable to the gap width between the shearing surfaces. They associated this "necklace" structure, similar to the current morphology at v = 20 μm/s, to a distortion of the velocity field in the presence of the walls. By comparison, binary polymer blend films (20% PS/PMMA) were also subjected to soft-shear dynamic zone annealing (DZA-SS) under the same conditions ($T_{max} \approx$ 180 °C, at v = 1, 20 and 60 μm/s). Figure 5 displays the AFM height images of the PS/PMMA blend films upon shear annealing by DZA-SS process. The PS phase was selectively removed by immersion into cyclohexane to enhance the contrast between the PS and PMMA phases. Similar to 20% AuPS/PMMA blend films, the binary polymer blends demonstrated a morphology transition from weakly deformed droplets, to "necklace-like" pattern of squashed domains, to highly elongated "strings" in the soft-shear direction as the translation speed increased.

To quantitatively compare soft-shear effect on NP-polymer and binary polymer blend films, the average domain aspect ratio (AR), domain size (S), and "string" width (W) were calculated by binarizing the TEM or AFM images, as listed in Table 1. At low translation speed range (v = 1 and 20 μm/s), the discrete domains were squashed and AR increased with increasing speed. The deformation trend is more pronounced for NP-polymer blends. The average domain size and string width in AuPS/PMMA blends were significantly smaller than that in PS/PMMA blends, which might be attributed to higher viscosity and surface tension modification due to the presence of multiple PS chains surrounding an Au core. Assuming the discrete elongated domains are ellipse-shaped, the average minor axis dimension (b) perpendicular to soft-shear direction can be extracted from S values and thereby also obtain the average domain widths (W =

2*b*). The correlation between *W* and translation speed is displayed in Figure 6 for 20% AuPS/PMMA and 20% PS/PMMA blend films. Generally, the average domain width decreases as the speed increases and the larger PS domain width at low speed gradually converges with the AuPS domain width at higher speed. In addition, the domain width distribution becomes narrower as *v* increases. Furthermore, soft-shear imposes a certain length scale on the highly stretched structure in shear direction, which is the characteristic inter-domain spacing (L^*).[21] The translation speed dependence of phase-separated morphology coarsening is quantitatively analyzed by 2D Fourier transformation (FFT) of TEM and AFM images. The characteristic inter-domain spacing (L^*) is determined from the maximum intensity wavenumber of the radial power spectrum. For both blends systems, increase in speed induced decrease in L^* because the equivalent annealing time above T_g is shortened (Figure 6). In accord with the domain width transition trends, AuPS/PMMA blend films show a shallower decrease to almost constant value of L^*, in contrast to the steep decline in PS/PMMA blend films as *v* increases.

To rationalize the soft-shear induced domain deformation transitions, the maximum shear rate ($\dot{\gamma}_{max}$) during one oscillatory shear period in DZA-SS process is estimated by $\dot{\gamma}_{max} = \tau_{max} / \eta_m$, where τ_{max} is the maximum shear stress and η_m is the viscosity of polymer matrix (i.e. PMMA). The maximum shear stress (τ_{max}) induced by thermal expansion mismatch of PDMS layer and polymer blend films has been previously estimated as $\tau_{max} \approx 12 \times 10^4$ Pa based on the equation $\tau_{max} = G_{PDMS} \times \varepsilon$, where G_{PDMS} is the shear modulus of PDMS and is ε is the maximum strain.[17] In the current blends systems, the molecular weights of PS ligands (M_n = 11.5 kg/mol) and PMMA matrix chains (M_n = 3.1 kg/mol) are lower than the entanglement molecular weights, respectively. [26,27] Consequently, the viscosities can be evaluated by zero shear rate viscosity, where $\eta_{PS\ (11.5k)} \approx 210$ Pa·s and $\eta_{PMMA\ (3.1k)} \approx 2680$ Pa·s at 180 °C. [27,28] Assuming the viscous

behavior of the blends is mainly responsible by the continuous matrix phase,[29] the maximum shear rate $\dot{\gamma}_{max} = \tau_{max} / \eta_{PMMA} \approx 45$ s^{-1}. When bulk immiscible blends are placed in a shear flow field, the deformation of the droplets is determined by the competition between interfacial tension (σ) and viscous shear stress (τ).[30] The interfacial tension tends to maintain spherical shaped droplets while shear stress exposes deformation trend in shear direction. The relative effect of viscous shear stress and interfacial tension is described by Capillary number, $Ca = \eta_m \dot{\gamma} R / \sigma$, where η_m, $\dot{\gamma}$, R, and σ denote matrix viscosity, shear rate, droplet radius, and interfacial tension, respectively.[31] When Ca exceeds critical Capillary number (Ca_{cr}), the droplets become unstable and break up, and the critical stable droplet radius is determined to be $R^* = \eta_m \dot{\gamma} / Ca_{cr} \sigma$.[32] For the current PS/PMMA blends, the viscosity ratio of dispersed phase to matrix phase is $\eta_{PS(11.5k)} / \eta_{PMMA(3.1k)} \approx 0.078$, and thus the critical Capillary number is estimated to be $Ca_{cr} \approx 0.67$. [31] Based on $\eta_{PMMA\ (3.1k)} \approx 2680$ Pa·s, $\dot{\gamma}_{max} \approx 45$ s^{-1} and $\sigma_{PS/PMMA} = 1.26$ mJ/m^2 at 180 ^{o}C, [33] the corresponding critical droplet radius is estimated to be $R^* \approx 7$ nm. However, the observed average elongated domain width is substantially larger than $2R^*$ (Figure 6). This discrepancy (stabilization of strings) is attributed to both shear flow and finite size effect. In the presence of shear flow, the varicose fluctuations of the elongated droplets can be convected away, thus suppressing the pressure differences and preventing Rayleigh instability growth.[34] Furthermore, thin film geometry also facilitates the formation of remarkably elongated "strings". Because the in-plane width of the elongated domains is larger than the film thickness (~ 90 nm), the 3D configuration of the domains is non-axisymmetric "ribbon-like" instead of axisymmetric "string-like". The varicose fluctuations induce non-axisymmetric sinusoidal thread configuration, which requires a higher wavelength distortion in order to generate a net decrease in surface area.[35]

Consequently, the highly elongated "ribbon" domains are stable with respect to capillary instability.

The above discussion only considered the influence of maximum shear rate ($\dot{\gamma}_{max}$) during DZA-SS process. However, the final microstructures of the blend films is not determined only by $\dot{\gamma}_{max}$, but also the full shear rate profile since the shear rate varies as temperature changes across the entire thermal gradient profile. Above T_g, the shear rate increases and decreases as temperature rises and falls, centered around T_{max} in response to the expansion and contraction of the PDMS capping layer.[17] The final morphology of AuPS or PS domains is determined by the integrated shear rate over one oscillatory DZA-SS shear cycle, which is correlated to the translation speed v. If the translation speed is sufficiently low (e.g. v = 20 μm/s), the phase separated domains will deform accordingly as the shear rate increases followed by a symmetric decrease, and after a shear cycle, slightly elongated domain morphology is observed. Upon increasing translation speed (e.g. v = 60 μm/s), the final morphology is reflective of a higher overall "effective" shear rate since the elongated structures get frozen as the blend film rapidly traverses the thermal profile. Further increase in translation speed may even generate less deformed structures as the blend systems cannot adjust the phase organization kinetics as fast as the shear rate variation. We then conclude that the variation of translation speed of the DZA-SS process can influence the "effective shear rate" ($\dot{\gamma}_E$) at the blend film surfaces and thus the phase-separated morphologies. While mainly a conceptual concept, the effective shear rate is essentially the determinant shear rate for the final observed morphologies over the course of the oscillatory shear cycle. The increase of translation speed from 1 μm/s to 60 μm/s induces a droplet- to-string transition for 20% AuPS/PMMA blend films confirming an increase of $\dot{\gamma}_E$ with DZA-SS speed. To gain further insights of how higher NP blend composition may be amenable

to such anisotropic sheared morphologies, DZA-SS processed 50% AuPS/PMMA blend films are investigated as a function of translation speed (varying effective shear rate). As shown in Figure 7a, 50% loading of nanoparticles relative to PMMA weight resulted in spinodal decomposition structures upon vacuum oven annealing at 180 ^{o}C for 16 h. The application of soft-shear then generated deformed spinodal structures as shown in Figure 7b. As v increased from 20 μm/s to 60 μm/s, the AuPS domains evolved into drastically elongated strings, indicating increasing $\dot{\gamma}_E$ with increasing translation speed. Simultaneously, the characteristic inter-domain spacing L^* decreased from ~ 1164 nm to ~ 332 nm. As v was raised to 120 μm/s and then to 140 μm/s, the unidirectional aligned structures were distorted again accompanied with increase in inter-domain spacing ($L^* \approx 703$ nm at $v = 120$ μm/s). This initially enhanced and then suppressed elongation of AuPS domains implies an increase followed by a decrease in effective shear rate. Furthermore, clearly, the effective shear rate variation dominates the phase separation scale instead of the corresponding annealing time, where higher $\dot{\gamma}_E$ induced smaller inter-domain spacing L^*.[21]

Conclusions

In summary, we studied simultaneous phase separation structure formation and deformation of a novel binary blend thin film system composed of AuPS nanoparticles and PMMA matrix under dynamic thermal gradient field induced soft-shear (DZA-SS). Progressive elongation of AuPS domains was achieved by adjusting the translation speed (v) and the correlation between translation speed, the effective shear rate determinant factor and the final blend film morphology was established. Remarkably unidirectional aligned nanoparticle strings were fabricated with the presence of soft-shear in confined thin film geometry. This soft-shear

directed nanoparticle assembly strategy can be easily adapted to other NP-polymer blend systems with roll-to-roll compatibility for production scale-up.

Methods

Poly (methyl methacrylate) (PMMA, M_n = 3.1 kg/mol, polydispersity=1.09) and polystyrene (PS, M_n = 11.5 kg/mol, polydispersity = 1.25) were purchased from Polymer Source Inc. and used as obtained. The thiol-polystyrene (PS-SH) grafted gold nanoparticles (AuPS) were synthesized by phase transfer reduction of [$AuCl^4$] in the presence of thiol ligands.[36] The average radius of gold core R_0 = 1.21 nm ± 0.42 nm. PS grafting density is 0.7 / nm^2. The thickness of the PS brush layer (M_n = 11.5 kg / mol) is R_n = 2.7 nm, calculated from interparticle distance assuming that the AuPS nanoparticles are closely packed. PMMA solutions (3 wt% in toluene) were admixed with appropriate amount of AuPS nanoparticles to generate blend solutions where the weight ratio of AuPS to PMMA is 20 % and 50 %. Separately, PS and PMMA solutions (both 3 wt% in toluene) were mixed together to generate 20% PS/PMMA solutions. The AuPS/PMMA and PS/PMMA solutions were flow coated into thin films on quartz substrates (G.M. Associates, Inc.). The quartz substrates were exposed to 1 h of ultraviolet-zone (UVO) treatment before flow coating. The film thickness (≈ 90 nm) was measured by interferometer (F-20 UV Thin Film Analyzer, Filmetrics, Inc.). AuPS/PMMA and PS/PMMA blend films were vacuum oven annealed at 50 °C for 6 h to remove residual solvent before further vacuum annealing or soft-shear dynamic zone annealing (DZA-SS). Upon vacuum oven annealing at 180 ^oC for 16 h, AuPS nanoparticles experienced subtle size increase (R_0 = 1.35 nm ± 0.48 nm) due to thermally instability of the thiol-Au bond.[18,37]

Sylgard-184, a two-part thermocurable poly (dimethyl siloxane) (PDMS) elastomer (Dow Corning Corp.), was used to make PDMS capping layer. A mixture of PDMS elastomer and

curing agent in 20:1 weight ratio was poured on glass slides and cured at 120 ^{o}C for 6 h. PDMS was then peeled off the glass slide to obtain ~0.5 mm thick smooth films. Shear stress was applied to the blend film surface by soft-shear dynamic zone annealing (DZA-SS) with $T_{max} \approx$ 180 °C at various translation speeds (v = 1, 20, 60, 120 and 140 μm/s). The procedure for DZA-SS experiments has been explained in detail in our previous papers.[17,38] After thermal annealing, the PDMS capping layer was removed and the blend film was further characterized. The nanoparticle distribution in these blend films were characterized with a JEOL JEM-1230 transmission electron microscopy (TEM) at 200 kV. Specimens for TEM were prepared by pre-coating a thin layer (≈ 10 nm) of aqueous poly(4-styrenesulfonic acid) (PSS; Sigma–Aldrich) solution on to the substrates prior to flow coating the blend films, annealing the multilayer films, and then floating the films by immersing into distilled water followed by transferring to copper grids. The surface topography of these blend films was imaged using a Dimension Icon atomic force microscope (AFM) (Bruker AXS) in tapping mode. Some of the annealed PS/PMMA blend films were immersed into cyclohexane for 30 min at room temperature to selectively remove the PS-rich domains.

Acknowledgements

We acknowledge the National Science Foundation *via* Grant NSF DMR-1411046 for support of this Cold Zone Annealing Soft-Shear study. MRB furthermore acknowledges funding by the National Science Foundation *via* DMR-1410845. The authors extend their sincere appreciation to the Deanship of Scientific Research at King Saud University for its funding of the Prolific Research group (PRG-1436-14). We are grateful to Dr. C. C. Han and Dr. K. B. Migler for valuable discussions.

References:

(1) Bockstaller, M. R.; Mickiewicz, R. A.; Thomas, E. L. *Advanced Materials* **2005**, *17*, 1331.

(2) Balazs, A. C.; Emrick, T.; Russell, T. P. *Science* **2006**, *314*, 1107.

(3) Ganesan, V.; Jayaraman, A. *Soft Matter* **2014**, *10*, 13.

(4) Ganesan, V.; Ellison, C. J.; Pryamitsyn, V. *Soft Matter* **2010**, *6*, 4010.

(5) Kao, J.; Thorkelsson, K.; Bai, P.; Rancatore, B. J.; Xu, T. *Chemical Society reviews* **2013**, *42*, 2654.

(6) Darling, S. B.; Yufa, N. A.; Cisse, A. L.; Bader, S. D.; Sibener, S. J. *Advanced Materials* **2005**, *17*, 2446.

(7) Bockstaller, M.; Thomas, E. *Physical Review Letters* **2004**, *93*.

(8) Kao, J.; Bai, P.; Lucas, J. M.; Alivisatos, A. P.; Xu, T. *J Am Chem Soc* **2013**, *135*, 1680.

(9) Gupta, S.; Zhang, Q.; Emrick, T.; Russell, T. P. *Nano Letters* **2006**, *6*, 2066.

(10) Gam, S.; Corlu, A.; Chung, H.-J.; Ohno, K.; Hore, M. J. A.; Composto, R. J. *Soft Matter* **2011**, *7*, 7262.

(11) Chung, H.-j.; Ohno, K.; Fukuda, T.; Composto, R. J. *Nano Letters* **2005**, *5*, 1878.

(12) Kumar, S. K.; Jouault, N.; Benicewicz, B.; Neely, T. *Macromolecules* **2013**, *46*, 3199.

(13) Meli, L.; Arceo, A.; Green, P. F. *Soft Matter* **2009**, *5*, 533.

(14) Mackay, M. E.; Tuteja, A.; Duxbury, P. M.; Hawker, C. J.; Van Horn, B.; Guan, Z.; Chen, G.; Krishnan, R. S. *Science* **2006**, *311*, 1740.

(15) Karim, A.; Slawecki, T. M.; Kumar, S. K.; Douglas, J. F.; Satija, S. K.; Han, C. C.; Russell, T. P.; Liu, Y.; Overney, R.; Sokolov, J.; Rafailovich, M. H. *Macromolecules* **1998**, *31*, 857.

(16) Wang, H.; Composto, R. J. *Macromolecules* **2002**, *35*, 2799.

(17) Singh, G.; Yager, K. G.; Berry, B.; Kim, H.-C.; Karim, A. *ACS Nano* **2012**, *6*, 10335.

(18) Zhang, R.; Singh, G.; Dang, A.; Dai, L.; Bockstaller, M. R.; Akgun, B.; Satija, S.; Karim, A. *Macromolecular Rapid Communications* **2013**, *34*, 1642.

(19) Russell, T. P.; Hjelm, R. P.; Seeger, P. A. *Macromolecules* **1990**, *23*, 890.

(20) Peter F. Green, H. O., Pinar Akcora, Sanat K. Kumar *Dynamics of Soft Matter* **2012**, 349.

(21) Derks, D.; Aarts, D. G. A. L.; Bonn, D.; Imhof, A. *Journal of Physics: Condensed Matter* **2008**, *20*, 404208.

(22) Hashimoto, T.; Matsuzaka, K.; Moses, E.; Onuki, A. *Physical Review Letters* **1995**, *74*, 126.

(23) Vermant, J.; Solomon, M. J. *Journal of Physics: Condensed Matter* **2005**, *17*, R187.

(24) Feng, J.; Joseph, D. D. *Journal of Fluid Mechanics* **1996**, *324*, 199.

(25) Migler, K. B. *Physical Review Letters* **2001**, *86*, 1023.

(26) Dobkowski, Z. *Rheol. Acta* **1995**, *34*, 578.

(27) O'Connor, K. M.; Scholsky, K. M. *Polymer* **1989**, *30*, 461.

(28) Majeste, J.-C.; Montfort, J. P.; Allal, A.; Marin, G. *Rheol. Acta* **1998**, *37*, 486.

(29) Wippler, C. *Polymer Bulletin* **1991**, *25*, 357.

(30) Taylor, G. I. *Proc. R. Soc. London A* **1932**, *138*.

(31) Tucker III, C. L., Moldenaers, P. *Annual Review of Fluid Mechanics* **2002**, *34*, 177.
(32) Pathak, J. A.; Migler, K. B. *Langmuir : the ACS journal of surfaces and colloids* **2003**, *19*, 8667.
(33) Carriere, C. J.; Biresaw, G.; Sammler, R. L. *Rheol. Acta* **2000**, *39*, 476.
(34) Frischknecht, A. *Physical Review E* **1998**, *58*, 3495.
(35) Son, Y.; Martys, N. S.; Hagedorn, J. G.; Migler, K. B. *Macromolecules* **2003**, *36*, 5825.
(36) Brust, M.; Walker, M.; Bethell, D.; Schiffrin, D. J.; Whyman, R. *Journal of the Chemical Society, Chemical Communications* **1994**, 801.
(37) Jia, X.; Listak, J.; Witherspoon, V.; Kalu, E. E.; Yang, X.; Bockstaller, M. R. *Langmuir : the ACS journal of surfaces and colloids* **2010**, *26*, 12190.
(38) Singh, G.; Yager, K. G.; Smilgies, D.-M.; Kulkarni, M. M.; Bucknall, D. G.; Karim, A. *Macromolecules* **2012**, *45*, 7107.

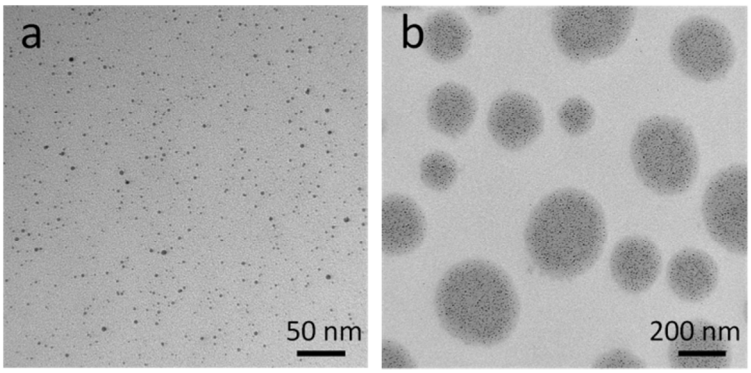

Figure 1. Top-view TEM micrographs of (a) as cast 20% AuPS/PMMA blend films and (b) phase-separated 20% AuPS/PMMA blend films after thermal annealing at 180 ^{o}C for 16 h. The dark circular domains are AuPS-rich domains while the light continuous phase is composed of PMMA.

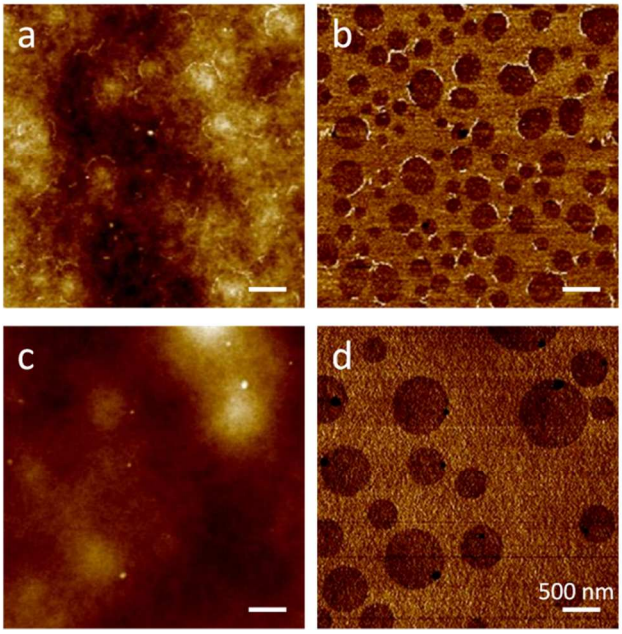

Figure 2. Comparison of 20% AuPS/PMMA (a, b) and 20% PS/PMMA (c,d) blend film phase-separated morphologies after thermal annealing at 180 ^{o}C for 16 h. (a) and (c) are AFM height images; (c) and (d) are corresponding AFM phase images.

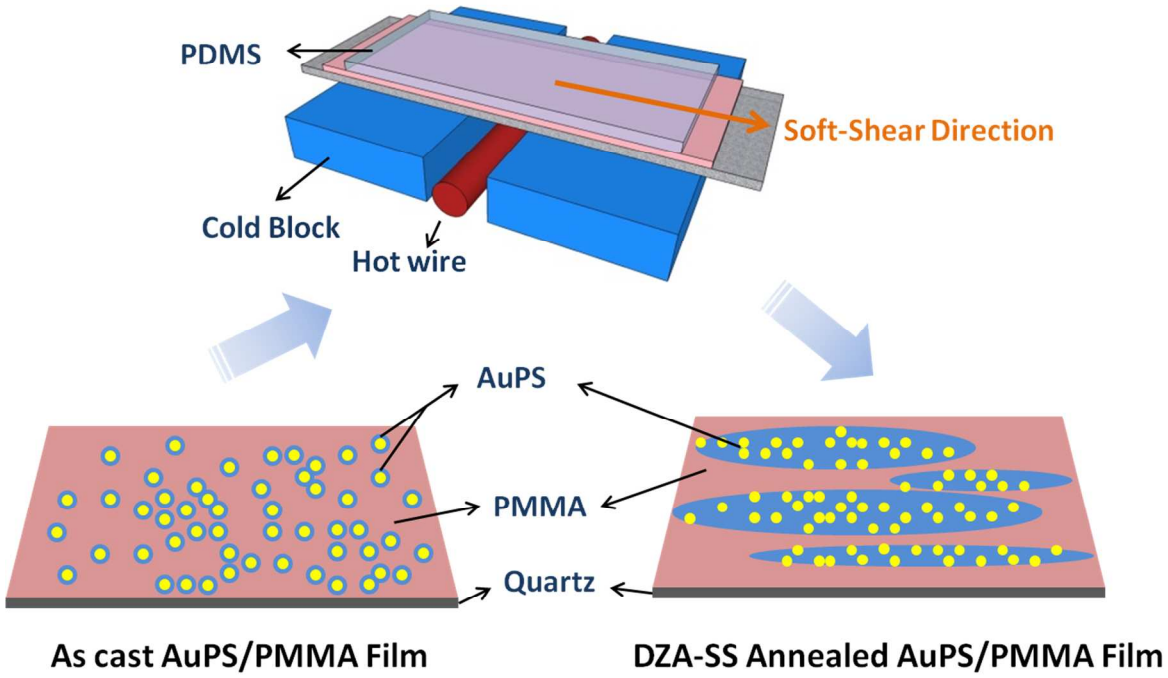

Figure 3. Schematic of soft-shear dynamic zone annealing (DZA-SS) process to generate unidirectional aligned elongated AuPS nanoparticle domain structures.

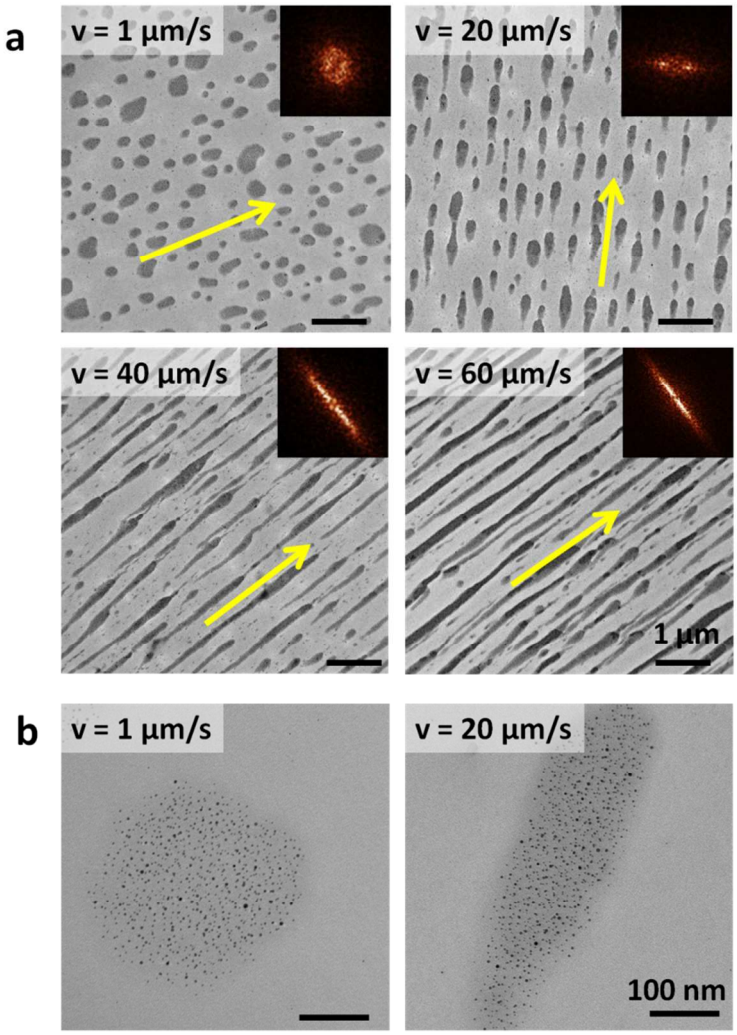

Figure 4. (a) Top-view TEM micrographs for DZA-SS induced morphologies of 20% AuPS/PMMA blend films processed at v = 1, 20, 40 and 60 μm/s. Arrow direction denotes soft-shear direction. The right corner insets are corresponding FFT images. (b) Zoom-in TEM micrographs of 20% AuPS/PMMA films processed at v = 1 and 20 μm/s.

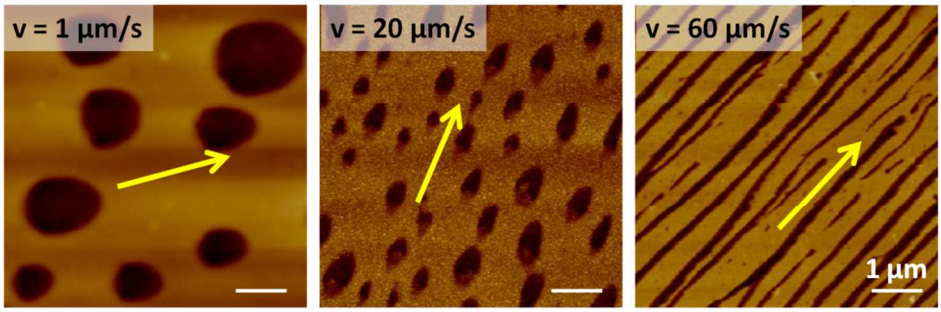

Figure 5. AFM height images for DZA-SS induced morphologies of 20% PS/PMMA blend films processed at v = 1, 20 and 60 µm/s. Arrow direction denotes soft-shear direction.

Table 1. Geometric characteristics comparison of DZA-SS processed blend films.

Characteristics	*AR*		*S* (µm^2)		*W* (nm)
v (µm/s)	1	20	1	20	60
20% AuPS/PMMA	1.43 ± 0.36	3.06 ± 1.11	0.064 ±0.041	0.053 ± 0.033	114 ± 16
20% PS/PMMA	1.72 ± 0.66	2.03 ± 0.84	0.79 ± 0.45	0.15 ± 0.10	161 ± 46

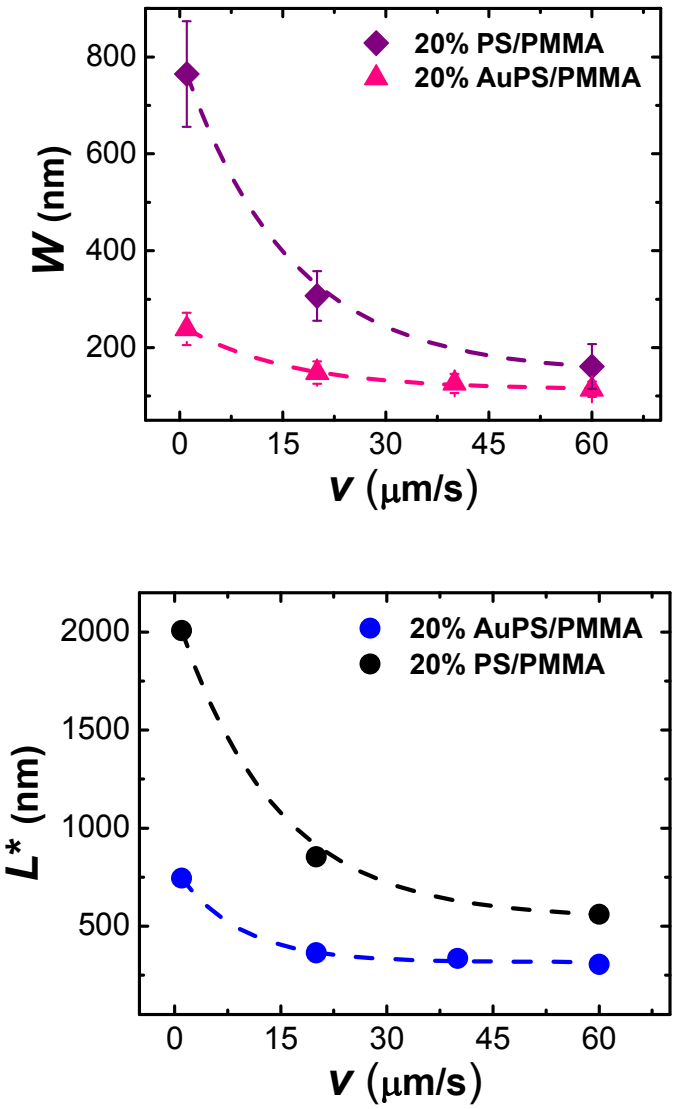

Figure 6. DZA-SS translation speed dependence of average domain width (W) orthogonal to soft-shear direction and characteristic inter-domain spacing (L^*) for 20% AuPS/PMMA and 20% PS/PMMA blend films.

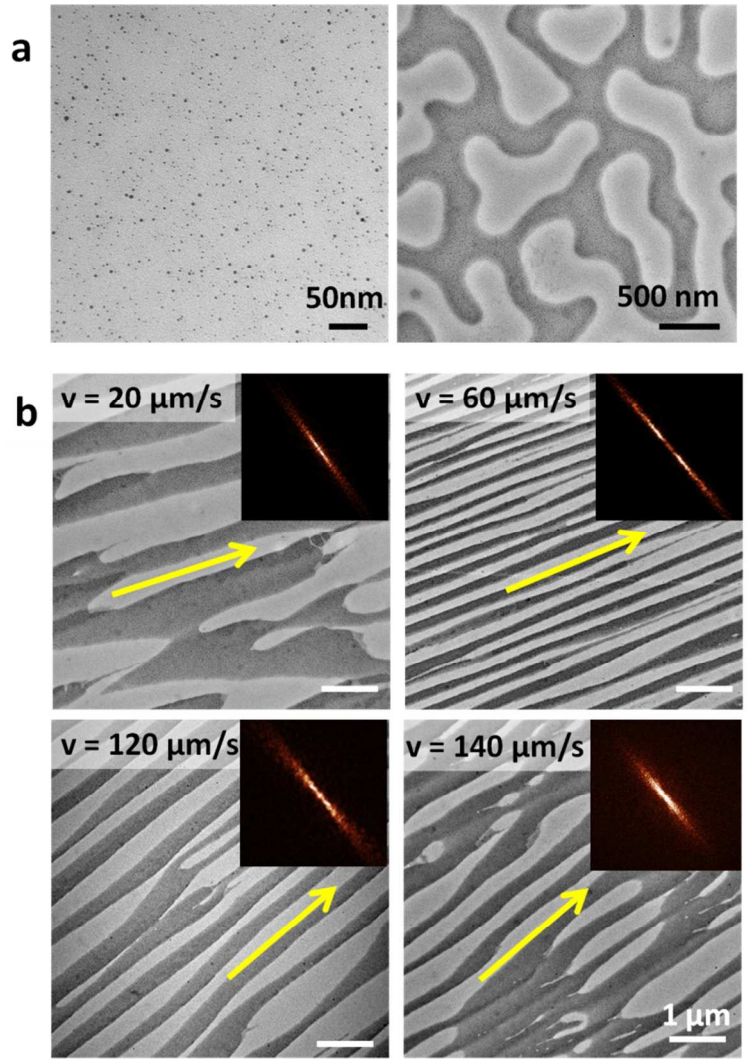

Figure 7. (a) Top-view TEM micrographs for as cast (left) and thermal annealed 50% AuPS/PMMA blend films at 180 ^{o}C for 16 h (right). (b) DZA-SS induced morphologies of 50% AuPS/PMMA blend films at v = 20, 60, 120 and 140 µm/s. Arrow direction denotes soft-shear direction. The upper corner insets are corresponding FFT images.